

# Mechanistic aspects of fracture and R-curve behavior in human cortical bone<sup>☆</sup>

R.K. Nalla<sup>a</sup>, J.J. Kruzic<sup>a</sup>, J.H. Kinney<sup>b</sup>, R.O. Ritchie<sup>a,\*</sup>

<sup>a</sup> *Materials Sciences Division, Lawrence Berkeley National Laboratory, and Department of Materials Science and Engineering, University of California, Berkeley, CA 94720, USA*

<sup>b</sup> *Lawrence Livermore National Laboratory, Livermore, CA 94550, USA*

Received 3 November 2003; accepted 4 February 2004

## Abstract

An understanding of the evolution of toughness is essential for the mechanistic interpretation of the fracture of cortical bone. In the present study, in vitro fracture experiments were conducted on human cortical bone in order to identify and quantitatively assess the salient toughening mechanisms. The fracture toughness was found to rise linearly with crack extension (i.e., rising resistance- or R-curve behavior) with a mean crack-initiation toughness,  $K_0$  of  $\sim 2 \text{ MPa}\sqrt{\text{m}}$  for crack growth in the proximal–distal direction. Uncracked ligament bridging, which was observed in the wake of the crack, was identified as the dominant toughening mechanism responsible for the observed R-curve behavior. The extent and nature of the bridging zone was examined *quantitatively* using multi-cutting compliance experiments in order to assess the bridging zone length and estimate the bridging stress distribution. Additionally, time-dependent cracking behavior was observed at stress intensities well below those required for overload fracture; specifically, slow crack growth occurred at growth rates of  $\sim 2 \times 10^{-9} \text{ m/s}$  at stress intensities  $\sim 35\%$  below the crack-initiation toughness. In an attempt to measure slower growth rates, it was found that the behavior switched to a regime dominated by time-dependent crack blunting, similar to that reported for dentin; however, such blunting was apparent over much slower time scales in bone, which permitted subcritical crack growth to readily take place at higher stress intensities.

© 2004 Elsevier Ltd. All rights reserved.

**Keywords:** Bone; Fracture; Tomography; R-curve; Toughening; Bridging; Microcracking

## 1. Introduction

The realization that bone mineral density alone cannot explain the therapeutic benefits of anti-resorptive agents in treating osteoporosis [1] has reemphasized the necessity of understanding how factors other than bone mineral density control fracture. Much of this renewed emphasis is being focused on mechanical properties that might affect fracture, like elastic modulus, strength, and toughness. Though there have been many studies on the mechanical properties of bone, specifically in terms of how such properties might vary with age and other

related factors, it is only recently that these properties have begun to be addressed quantitatively with regard to the microstructure of the tissue (e.g., [2–18]). Indeed, human bone has a complex hierarchical microstructure [3,4,19] that can be considered at several dimensional scales [3]. At the shortest length-scale, it is composed of type-I mineralized collagen fibers (up to 15  $\mu\text{m}$  in length, 50–70 nm in diameter) bound and impregnated with carbonated apatite nanocrystals (tens of nm in length and width, 2–3 nm in thickness) [3]. These fibers are further organized at a microstructural length-scale into a lamellar structure with roughly orthogonal orientations of adjacent lamellae (3–7  $\mu\text{m}$  thick) [4]. Permeating this lamellar structure are the secondary osteons [19] (up to 200–300  $\mu\text{m}$  diameter): large vascular channels (up to 50–90  $\mu\text{m}$  diameter) oriented roughly along the longer axis of the bone shaft and surrounded by circumferential lamellar rings, with so-called “cement lines” at the outer boundary. The difficulty in understanding the mechanisms of fracture in bone clearly lies in determining the

<sup>☆</sup>This work was supported in part by the National Institutes of Health under Grant No. 5R01 DE015633 (for RKN and JHK), and by the Director, Office of Science, Office of Basic Energy Science, Division of Materials Sciences and Engineering of the Department of Energy under Contract No. DE-Ac03-76SF00098 (for JJK and ROR).

\*Corresponding author. Tel.: +1-510-486-5798; fax: +1-510-486-4881.

E-mail address: [roritchie@lbl.gov](mailto:roritchie@lbl.gov) (R.O. Ritchie).

relative importance of these microstructural hierarchies on crack initiation, subsequent crack propagation and consequent unstable fracture, and in separating their effects on the critical fracture events. Such an understanding is of vital importance from the perspective of developing a realistic framework for fracture risk assessment, and for determining how its increasing propensity for fracture with age or disease can be prevented.

## 2. Background

With respect to the fracture resistance, there is now a large body of work available in the literature aimed at determining the fracture toughness of cortical bone, mainly in terms of the critical stress intensity,  $K_c$ <sup>1</sup> (e.g., [21–25]). While the use of  $K_c$  as a single-value measure of the toughness is appropriate for many materials, in some cases the fracture resistance actually increases with crack extension, promoting stable crack growth and requiring a resistance-curve (R-curve) fracture-mechanics approach [20,26]. In particular, R-curves are necessary to describe the fracture resistance of materials toughened by crack-tip shielding [27–29], i.e., by extrinsic toughening mechanisms<sup>2</sup> such as crack bridging, constrained microcracking, or in situ phase transformations, which develop in the crack wake as the crack extends. In such instances, crack extension commences at a *crack-initiation toughness*,  $K_0$ , while sustaining further crack extension requires higher driving forces until typically a “plateau” or steady-state toughness is reached. The corresponding slope of the R-curve can be considered as a measure of the *crack-growth toughness*.

Prevailing evidence suggests that extrinsic shielding mechanisms are primarily responsible for the in vitro toughness of mineralized tissues, which results in corresponding R-curve behavior [7,13,14,16,30–35]. Specific mechanisms that have been observed include microcracking in bone [7,16,30] and dentin [34], bridging by collagen fibers and by uncracked ligaments in bone and dentin [14,31–35], and crack deflection

due to crack–osteon interactions in bone [14], all mechanisms that illustrate the critical role of microstructure in controlling the fracture properties of these materials. However, the mere observation of these mechanisms does not ensure that they provide a meaningful contribution to the toughness; additional experiments are necessary to verify and quantify their significance.

Recent studies have provided strong experimental evidence that crack bridging [14,32], rather than constrained microcracking [7,30], may be a major source of crack-growth toughness (and hence, rising R-curve behavior) in human cortical bone; similar results have been reported by other investigators for bovine bone [33]. The prime source of such bridging in human bone appears to be from the formation of uncracked ligaments in the crack wake, which are created either by the non-uniform advance of the crack front and/or by the imperfect linking of microcracks ahead of the crack tip with the main crack [14,32]. From a mechanics perspective, such crack bridging acts to reduce the stress intensity experienced at the crack tip,  $K_{tip}$ , relative to the applied stress intensity,  $K_{app}$ , by an amount typically referred to as the bridging stress intensity,  $K_{br}$ , viz.:

$$K_{tip} = K_{app} - K_{br}. \quad (1)$$

The reduction in stress intensity is a due to the fact that bridges in the crack wake sustain a portion of the applied load that would otherwise contribute to crack-growth. Since bridges develop with crack extension,  $K_{br}$  increases with crack extension as well, resulting in rising R-curve behavior. A steady-state “plateau” toughness may be reached under conditions where bridges are created and destroyed at the same rate, at which point  $K_{br}$  essentially becomes constant. Accordingly, within this framework, a major goal of the present work is to present new experimental results that (i) confirm the prominent role of uncracked-ligament bridging in the toughening of human cortical bone in the context of the underlying microstructure, and (ii) provide a more quantitative description of the bridging zone which lies in the crack wake.

Because bone is a load-bearing tissue in vivo, there is definite concern that time-dependent (subcritical) crack growth may occur at sustained (quasi-static) loads less than those required to cause instantaneous (overload) fracture, i.e., at stress intensities less than the fracture toughness,  $K_c$ . To our knowledge, this issue has rarely been addressed in cortical bone. However, in dentin, which is microstructurally a simplified analog of bone, such subcritical crack growth has been reported in vitro under sustained loads, with hydrated dentin showing comparatively less susceptibility to such cracking due to significant time-dependent crack-tip deformation (blunting), compared to dehydrated dentin where relatively little blunting occurs [31]. Thus, another goal of this

<sup>1</sup>The fracture toughness,  $K_c$ , is the critical value of the stress intensity,  $K$ , for unstable fracture at a pre-existing crack, i.e., when  $K = Y\sigma_{app}(\pi a)^{1/2} = K_c$ , where  $\sigma_{app}$  is the applied stress,  $a$  is the crack length, and  $Y$  is a function (of order unity) of crack size and geometry. Alternatively, the toughness can be expressed as a critical value of the strain energy release rate,  $G_c$ , defined as the change in potential energy per unit increase in crack area, where  $G_c = K_c^2/E'$ , with  $E'$  as the appropriate elastic modulus [20].

<sup>2</sup>Crack propagation can be considered as a mutual competition between two classes of mechanisms: *intrinsic* mechanisms, which are microstructural damage mechanisms that operate ahead of the crack tip, and *extrinsic* mechanisms, which act to “shield” the crack from the applied driving force and operate principally in the wake of the crack tip [27–29].

work is to discern whether such time-dependent crack-ing and crack-blunting behavior can also occur in human cortical bone.

### 3. Materials and methods

#### 3.1. Materials

Fresh frozen human cadaveric humeral cortical bone from three donors (34–41 years old) was used in this study. Blocks of bone were obtained by carefully sectioning the medial cortices of the mid-diaphyses of the humeri. Thirteen ( $N = 13$ ) compact-tension, C(T), specimens, with specimen thicknesses,  $B \sim 1.2$ – $3.3$  mm, widths,  $W \sim 13$ – $18.3$  mm and initial crack lengths,  $a \sim 3.1$ – $5.5$  mm, were machined<sup>3</sup> from these blocks;  $N = 1$  were from a 34-year old female,  $N = 8$  from a 37-year old male, and  $N = 4$  from a 41-year old female. The samples were all orientated with the starter notch and the nominal crack-growth direction along the proximal–distal direction of the humerus (in the longitudinal–radial plane), i.e., parallel to the long axis of the osteons and hence, the long axis of the humerus. These specimens were polished to a 1200 grit finish, followed by polishing steps using a 1  $\mu$ m alumina suspension and finally a 0.05  $\mu$ m alumina suspension. The notch was introduced using a slow ( $\sim 100$  RPM) speed saw (TechCut II, Allied High Tech Products, Inc., Rancho Dominguez, CA), and finally, razor-micronotched (root radius,  $\rho \sim 15$   $\mu$ m, micronotch depth  $\sim 100$   $\mu$ m), where the razor-micronotch was created by repeatedly sliding a razor blade over the saw-cut notch using a custom-made rig, while continually irrigating with a 1  $\mu$ m diamond slurry.

#### 3.2. R-curve testing

R-curves were measured to evaluate the resistance to fracture in terms of the stress intensity,  $K$ , as a function of crack extension,  $\Delta a$ , under a monotonically increasing driving force. The C(T) specimens ( $N = 7$ : mean age in years = 37.71 (SD = 2.5), see Table 1 for further details) were prepared prior to testing by soaking in Hanks' Balanced Salt Solution (HBSS) for at least 40 h at room temperature in air-tight containers.<sup>4</sup> Tests were then conducted in ambient air (25°C, 20–40% relative humidity) with the specimens being continuously irrigated with HBSS. The specimens were loaded in

Table 1  
Resistance curve behavior of human cortical bone

Donor information <sup>a</sup>	Initiation toughness $K_0$ (MPa $\sqrt{m}$ )	Slope (MPa $\sqrt{m/mm}$ )	Coefficient of determination ( $R^2$ )
34FL	2.12	0.31	0.98
37ML#1	1.69	0.50	0.88
37ML#2	2.20	0.28	0.97
37MR#1	2.07	0.49	0.97
37MR#2	1.85	0.41	0.94
41FL#1	2.07	0.41	0.97
41FL#2	2.23	0.34	0.96

<sup>a</sup>The notation reads as follows: age (years), sex (M = male, F = female), arm (L = left, R = right), with any subsequent number being a unique identifier when more than one specimen were taken from the same location.

displacement control using standard servo-hydraulic testing machines (MTS 810, MTS Systems Corporation, Eden Prairie, MN) with a loading rate of  $\sim 0.015$  mm/s (to simulate quasi-static loading conditions) until the onset of cracking, which was determined by a drop in load, or non-linearity in the load–displacement curve. At this point, the sample was unloaded by 10–20% of the peak load to record the sample load-line compliance at the new crack length using a linear variable-displacement transducer (LVDT) mounted in the load frame. This process was repeated at regular intervals until the end of the test, at which point the compliance and loading data were analyzed to determine the fracture resistance,  $K_R$ , as a function of crack extension,  $\Delta a$ . Crack lengths,  $a$ , were calculated from the compliance data obtained during the test using standard C(T) load-line compliance calibrations [37]:

$$a/W = 1.0002 - 4.0632U + 11.242U^2 - 106.04U^3 + 464.33U^4 - 650.68U^5, \quad (2)$$

where  $U$  is a fitting function, written as

$$U = \frac{1}{(FC)^{1/2} + 1}. \quad (3)$$

Here  $C$  is the ideal, bridge-free, sample compliance, and  $F$  is a calibration constant, taken to be that which gives the best agreement between the initial compliance and crack length at the beginning of the test. Due to crack bridging, discrepancies invariably occurred between the ideal compliance,  $C$ , and the measured compliance,  $C_m$ . Accordingly, re-normalization to the actual crack length was periodically achieved using optical microscopy to directly measure the crack length,  $a$ . Differences between the compliance and optically measured crack length were corrected by assuming that any such error accumulated linearly with crack extension.

After R-curve testing, crack paths were examined using optical microscopy and scanning electron microscopy (SEM) in order to observe the interaction of the

<sup>3</sup>The specimens were machined using a standard mill, with the bone being kept moist throughout the machining process.

<sup>4</sup>It is possible that there might be some degradation of the collagen phase, which can result in changes in properties with time. However, in a parallel investigation of dentin, a structurally simpler analog of bone, no such changes could be detected following short time storage under similar conditions [36].

crack with microstructural features and the relevant toughening mechanisms.

### 3.3. X-ray computed tomography

Because the stress-state is quite different in the interior of a sample undergoing inelastic deformation as compared to its surface (the surface is in a state of plane stress whereas the interior, with sufficient constraint, is in plane strain), and this varying degree of stress triaxiality has a profound effect on fracture properties (e.g., see Ref. [20]), it is important to observe cracking behavior both at the surface and within the bulk of the sample to determine if the same toughening mechanisms exist throughout the specimen. To accomplish this, synchrotron X-ray computed tomography was performed on two of the tested specimens (34FL and 37ML#2) at the Stanford Synchrotron Radiation Laboratory (SSRL), Menlo Park, CA, to investigate the extent of bridging throughout the thickness of the specimen. Imaging was performed with monochromatic 25 keV X-rays, with a voxel size (spatial resolution) of  $\sim 5 \mu\text{m}$  and exposure times of  $\sim 10$  min for every 1 mm of crack length. The tomography data were reconstructed into three-dimensional images by a Fourier-filtered back-projection algorithm; further details of this technique are well described elsewhere [38].

### 3.4. Multi-cutting compliance experiments

To quantitatively assess the extent and nature of the bridging zone behind the crack tip, a multi-cutting compliance technique, similar to that of Wittmann and Hu [39–41], was used for three post R-curve tested specimens ( $N=3$ : 37ML#1, 37MR#2, and 41FL#1). Specifically, a diamond saw blade was employed to sequentially cut out the crack and thus incrementally eliminate the crack wake (in steps of  $\sim 0.25$ – $1$  mm), while the sample compliance was measured (using the LVDT in the test frame) after each incremental saw cut. The width of cut ( $\sim 300 \mu\text{m}$ ) has negligible influence on the compliance. When the portion of the crack wake that is eliminated is traction-free, there is no change in compliance after cutting, i.e., the saw cut notch behaves as a bridge-free crack. However, if active bridges are eliminated from the crack wake by the saw blade, a corresponding increase in the sample compliance is expected. By using this technique, the bridging zone length,  $L$ , can be assessed by noting the notch length when the sample compliance begins to increase. Furthermore, a normalized bridging stress distribution can be estimated from the multi-cutting compliance data using [41]:

$$\frac{\sigma_{\text{br}}(x)}{\sigma_{\text{max}}} = \frac{C^2(a)C'_m(x)}{C_m^2(x)C'(a)}, \quad (4)$$

where  $a$  is the crack length,  $C$  is the ideal, bridge-free, compliance,  $C_m(x)$  is the measured compliance after cutting to the position  $x$  measured from the load line, and  $C'(z) = dC(z)/dz$ . The bridging stress distribution,  $\sigma_{\text{br}}(x)$ , obtained from the multi-cutting compliance data is normalized by the factor  $\sigma_{\text{max}}$ , which corresponds to the maximum bridging stress at the crack tip. The ideal compliance may be computed for any given crack length using the relation [37]:

$$C = \frac{1}{E} \left( \frac{1+a/W}{1-a/W} \right)^2 (2.1630 + 12.219a/W - 20.065(a/W)^2 - 0.9925(a/W)^3 + 20.609(a/W)^4 - 9.9314(a/W)^5), \quad (5)$$

where all the variables in the equation have been defined previously.

Alternatively, one may assume a commonly used bridging function a priori in order to estimate the bridging stress distribution [42–46], viz.:

$$\frac{\sigma_{\text{br}}}{\sigma_{\text{max}}} = \left( 1 - \frac{X}{L} \right)^p, \quad (6)$$

where  $X$  is the distance behind the crack tip ( $X = a - x$ ), and  $p$  is an exponent that describes the shape of the bridging stress distribution as it decreases from  $\sigma_{\text{max}}$  at the crack tip to zero at  $X = L$ . The exponent,  $p$ , may be determined from the compliance data using the relation [44]:

$$\frac{L}{p+1} = \frac{C(a)}{C'(a)} \left( \frac{C(a)}{C_m(a)} - 1 \right) \quad (7)$$

where all symbols have been previously defined.

In order to further quantify the bridging stresses, it must first be noted that the bridging stress distribution,  $\sigma_{\text{br}}$ , may be related to the bridging stress intensity,  $K_{\text{br}}$ , by the relationship [47,48]:

$$K_{\text{br}} = \int_0^a h(a, x) \sigma_{\text{br}} dx, \quad (8)$$

where  $x$  is the position measured from the load line,  $a$  is the crack length, and  $h(a, x)$  is a geometry-dependent weight function, derived for the C(T) geometry to be [48]:

$$h = \sqrt{\frac{2}{\pi a}} \frac{1}{\sqrt{1-x/a}} \left[ 1 + \sum_{(v,\mu)} \frac{A_{v\mu}(a/W)^\mu}{(1-a/W)^{3/2}} (1-x/a)^{v+1} \right]. \quad (9)$$

The coefficients  $A_{v\mu}$  may be found in Ref. [48];  $W$  refers to the sample width. By combining Eqs. (4), (8) and (9), or Eqs. (6), (8) and (9), the unknown  $\sigma_{\text{max}}$  may be found for each proposed bridging function provided the bridging stress intensity,  $K_{\text{br}}$ , is known.

### 3.5. Time-dependent cracking/blunting experiments

In many materials, cracks can propagate subcritically, i.e., at stress intensities less than  $K_c$ , under the action of sustained loads; however, such time-dependent crack growth can be inhibited or even arrested by blunting at the crack tip. In order to assess whether human cortical bone experiences such time-dependent cracking or crack-blunting phenomena, five C(T) specimens ( $N = 5$ : mean age in years = 38.3 (SD = 2.07), see Table 3 for further details) were tested under constant displacement conditions using standard servo-hydraulic testing machines (MTS 810, MTS Systems Corporation, Eden Prairie, MN) at 37°C while immersed in HBSS. The specimens were loaded under displacement control until the R-curve initiation toughness was slightly exceeded, after which the load–line displacement was held fixed. Additionally, in order to make further direct observations of the time-dependent cracking and blunting behavior, a similar experiment ( $N = 1$ : 41FL#4) was conducted at 25°C in ambient air using an in situ loading fixture in an optical microscope while continuously irrigating the specimen with HBSS. Constant-displacement conditions were used for these tests due to the fact that under such conditions, a growing crack experiences decreasing stress intensity with crack extension,

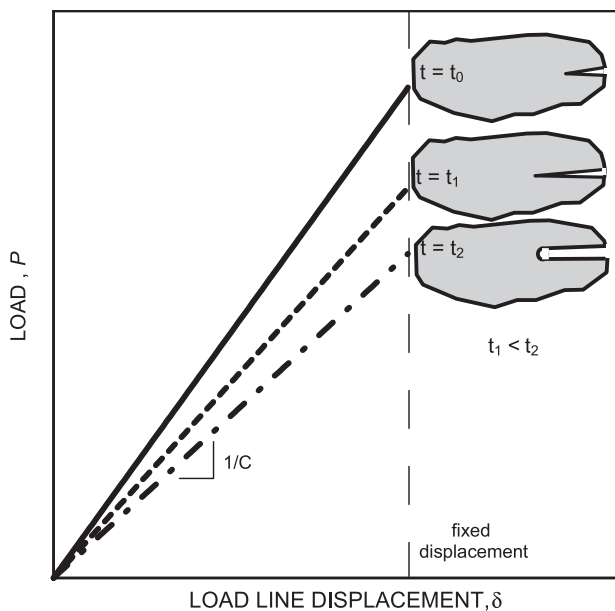


Fig. 1. Idealized schematic illustrating how load vs. time data can be converted into compliance vs. time data for a constant displacement test. In this example, the solid line represents the initial sample compliance ( $C$ ) curve at  $t = t_0$ , while the dashed lines at  $t = t_1$  and  $t = t_2$  ( $t_1 \ll t_2$ ) represent the compliance curves associated with the measured loads at  $t = t_1$  and  $t = t_2$ . By measuring the load drop with time, the crack-growth behavior (as schematized by the insets) may be inferred for short time scales ( $t_0$  to  $t_1$ ). Crack blunting becomes significant at longer time scales ( $t_2$ ), when additional load drop at constant displacement does not correlate with change in crack length. The insets at each time,  $t$ , show a schematic of the crack.

and thus stable crack growth is achievable. During the test, the load was monitored as a function of time, with a drop in load indicating that either crack extension or crack blunting had occurred (Fig. 1). In order to distinguish between the two, the test was periodically interrupted in order to make direct observations of the crack using optical microscopy. For the case of crack extension with minimal blunting, the load versus time data may be converted into crack length versus time data using the above compliance calibration (Eqs. (2) and (3)), assuming a linear compliance curve with fixed origin (Fig. 1—from  $t = t_0$  to  $t_1$ ). As described above for R-curve measurements, the actual crack length was periodically verified by optical microscopy and any errors in the crack length due to bridging were corrected by assuming such errors accumulated linearly with crack extension.

## 4. Results

### 4.1. Resistance-curve behavior

As noted above, the fracture toughness of bone is best represented in terms of R-curves. Accordingly, in vitro load–displacement data (e.g., Fig. 2a) were analyzed to evaluate the resistance to fracture in terms of the stress intensity,  $K$ , as a function of crack extension,  $\Delta a$ . The resulting R-curves for hydrated cortical bone are shown in Fig. 2b. Cracks can be seen to grow subcritically for between 5 and 7 mm during the course of each test. The average crack-initiation toughness,  $K_0$ , obtained by extrapolating a linear fit of the data for each sample to  $\Delta a = 0$ , was 2.03 (SD = 0.19)  $\text{MPa}\sqrt{\text{m}}$  with the R-curves monotonically rising with a mean slope of 0.39 (SD = 0.09)  $\text{MPa}\sqrt{\text{m}/\text{mm}}$ ; individual values are listed in Table 1.

In order to consider these measured toughnesses as lower-bound, geometry-independent values, it is noted that a condition of plane strain is required. According to ASTM Standard E-399, this is achieved when the sample thickness is greater than  $2.5(K/\sigma_y)^2$ , i.e., the thickness is significantly larger than the plastic or damage zone size of  $r_y \sim 1/2\pi (K/\sigma_y)^2$ , where  $\sigma_y$  is the yield strength or more appropriately the stress to cause inelastic deformation. For cortical bone, using a value of  $\sigma_y \sim 80 \text{ MPa}$  [49], this requires sample thicknesses greater than  $\sim 1$  to 10 mm to yield plane-strain conditions for the range toughness values observed on the R-curves, i.e., 2–5  $\text{MPa}\sqrt{\text{m}}$ . It is also to be noted that the specimen thicknesses used here (1.2–3.3 mm) were sometimes lower than the 2–3 mm suggested by Norman et al. [23] for plane strain in human bone. However, as the ASTM criterion is generally quite conservative and the damage zone, as estimated from plastic zone calculations [50], was well-contained within the specimen

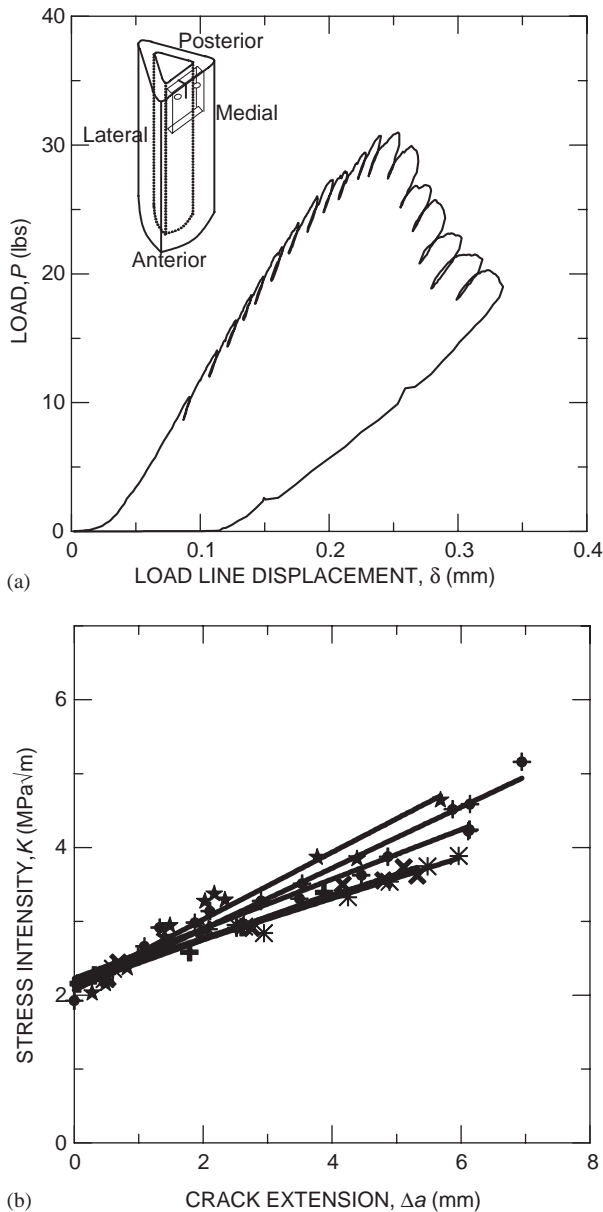


Fig. 2. (a) Typical load vs. load-line displacement curve, and (b)  $K_R(\Delta a)$  resistance-curves for stable crack extension in hydrated cortical bone. Each data point represents a partial unloading event during the test. Note the linearly rising R-curve behavior. The inset in (a) schematically shows the anatomical orientation that the specimens were taken from the humeri.

boundaries, it is believed that in the current tests, conditions close to plane strain were maintained. Furthermore, experiments by Behiri and Bonefield [51] showed no specimen thickness dependence on the fracture toughness of bovine tibia down to thicknesses of 500  $\mu\text{m}$  for the same longitudinal fracture orientation.

#### 4.2. Crack-path observations

The R-curve tests also allowed for stable crack extension, making it possible to directly observe for

relevant toughening mechanisms and their relationship to the salient features of the microstructure of bone. Fig. 3 shows an example of typical crack growth from the notch in a hydrated cortical bone specimen. The discontinuous nature of the crack path in the optical micrograph in the center of the figure indicates extensive formation of uncracked ligaments (indicated by white arrows) behind the crack tip and consequent “out-of-plane” deflection of the crack. On the sample surface, such ligaments, some as large as hundreds of micrometers in size, can be readily seen to “bridge” the crack, as also observed in earlier studies [14,32]. Furthermore, the X-ray tomography results in Fig. 3 (lower section) confirm that such uncracked ligaments occur throughout the bulk of the specimens, and are not an artifact of the surface stress state. Fig. 3 (lower section) shows four reconstructed through-thickness (two-dimensional) slices at different positions in the same specimen; again, the existence of extensive ligaments (as indicated by white arrows) throughout the bulk of the material is apparent. From these latter images, it is evident that these bridges are not continuous throughout the sample thickness. Further definitive *visual* evidence is seen in the three-dimensional reconstructions for a section of the same crack as shown in Fig. 4. It is interesting to note from both two- and three-dimensional tomography that the crack does not penetrate the osteon at any stage. Indeed, the path taken by the crack for this orientation appears to be dictated by the *interface* of the osteonal system with the surrounding matrix, i.e. the cement line.

#### 4.3. Multi-cutting compliance experiments

Based on crack path observations, crack bridging along the crack flanks appears to be the primary mechanism responsible for the R-curve behavior in bone. To quantify such bridging, measurements were made of the elastic compliance of the samples, as detailed in Section 3.4. The results of the multi-cutting compliance experiments for one of the R-curve specimens (41FL#1) are shown in Fig. 5, while the other two specimens (37ML#1 and 37MR#2) showed similar behavior. Each data point in Fig. 5 indicates the mean of five compliance measurements for the corresponding notch length, while the line through the data points indicates a best-fit sixth-order polynomial function to the data. Also shown for comparison are the (theoretical) compliance curves for the bridge-free cracked material and for the uncracked material, the latter corresponding to Eq. (5). As reported previously for both dentin and bone [14,32], it is evident that the experimentally measured compliance values are lower than that for the ideal, unbridged crack, providing direct evidence to the notion of bridging as a definitive extrinsic toughening mechanism in cortical bone. Note that had constrained microcracking been the dominant

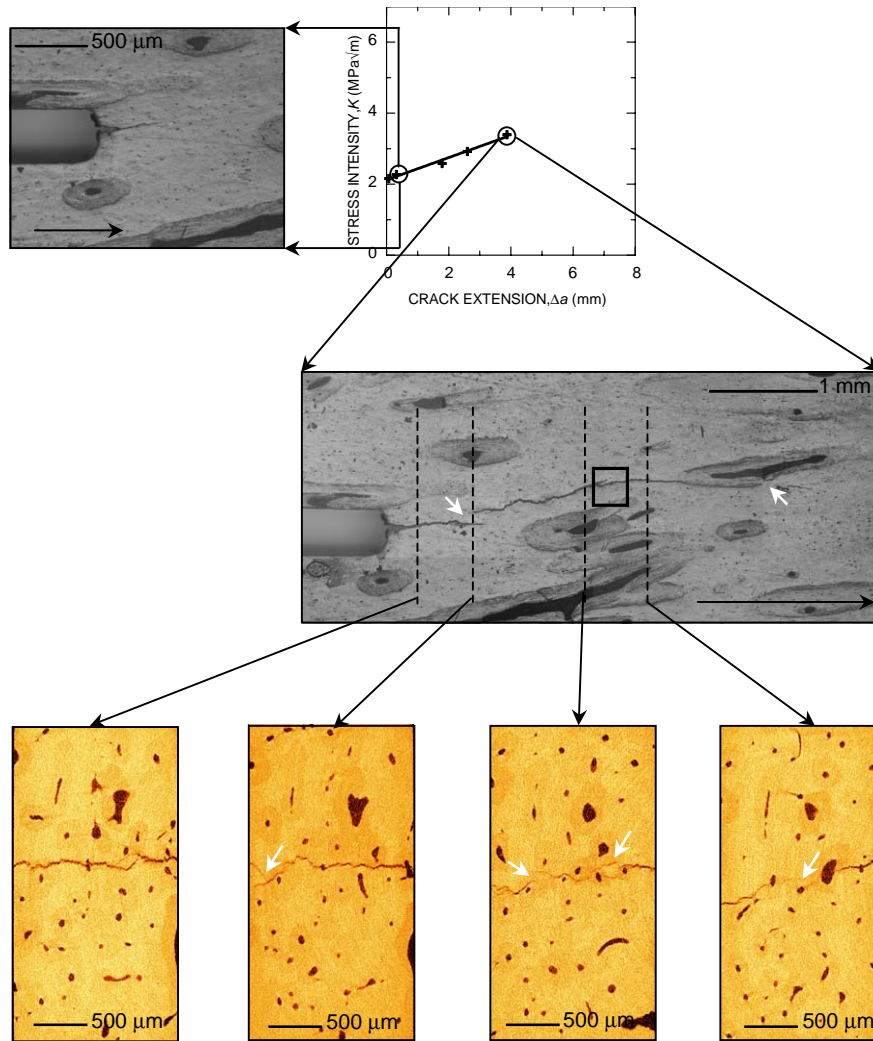


Fig. 3. Typical optical micrographs of stable crack growth in 34-year old human cortical bone are shown together with the corresponding R-curve. An optical micrograph (center) together with tomographic through-thickness slice-wise reconstructions (below) clearly support the presence of uncracked ligaments (indicated by white arrows) in the crack wake. The black arrows in the optical micrographs give the direction of nominal crack growth.

toughening mechanism, the measured compliance values would be expected to be higher [32]. Furthermore, Fig. 5 shows that essentially no increase in the sample compliance was observed during removal of the crack wake until the saw-cut notch reached within  $\sim 5.5$  mm of the crack tip. This indicates that the bridging-zone length,  $L$ , is on the order of 5.5 mm for sample 41FL#1, while similar values of 5 and 5.8 mm were found for samples 37ML#1 and 37MR#2, respectively. Applying Eqs. (4) and (6), two different estimates of the normalized bridging stress distribution may be obtained by using the best-fit polynomial function to the measured compliance data (e.g., Fig. 5). A summary of these results for all three samples can be seen in Table 2, while a plot comparing the stress distributions is shown in Fig. 6.

Values for  $\sigma_{\max}$  in Table 2 and Fig. 6 were obtained by noting that an estimate for  $K_{br}$  can be made from the R-

curve data through the use of Eq. (1). Indeed, recognizing that the near-tip criteria for crack advance is  $K_{ip} = K_0$ , the additional (crack-growth) contribution to the toughness is due to the term  $K_{br}$ . According to the results in Table 2, the bridging zone should have been saturated after about 5–5.8 mm of crack extension, giving a “plateau” (steady-state) toughness on the R-curve beyond that point. While no distinct “plateau” toughness was observed in the present samples, this may be attributed to the small sample size; indeed, larger samples would be needed to demonstrate such a plateau region and avoid effects of finite sample size, e.g., Ref. [52]. For each sample, the measured toughness values at  $\Delta a = L$  was used to estimate  $K_{br}$  by subtracting the initiation toughness (Table 1), from the total fracture resistance,  $K_{app}$  (Eq. (1)). The values used for each sample are again summarized in Table 2. Thus, based on these approximate values for  $K_{br}$ ,  $\sigma_{\max}$  is deduced to

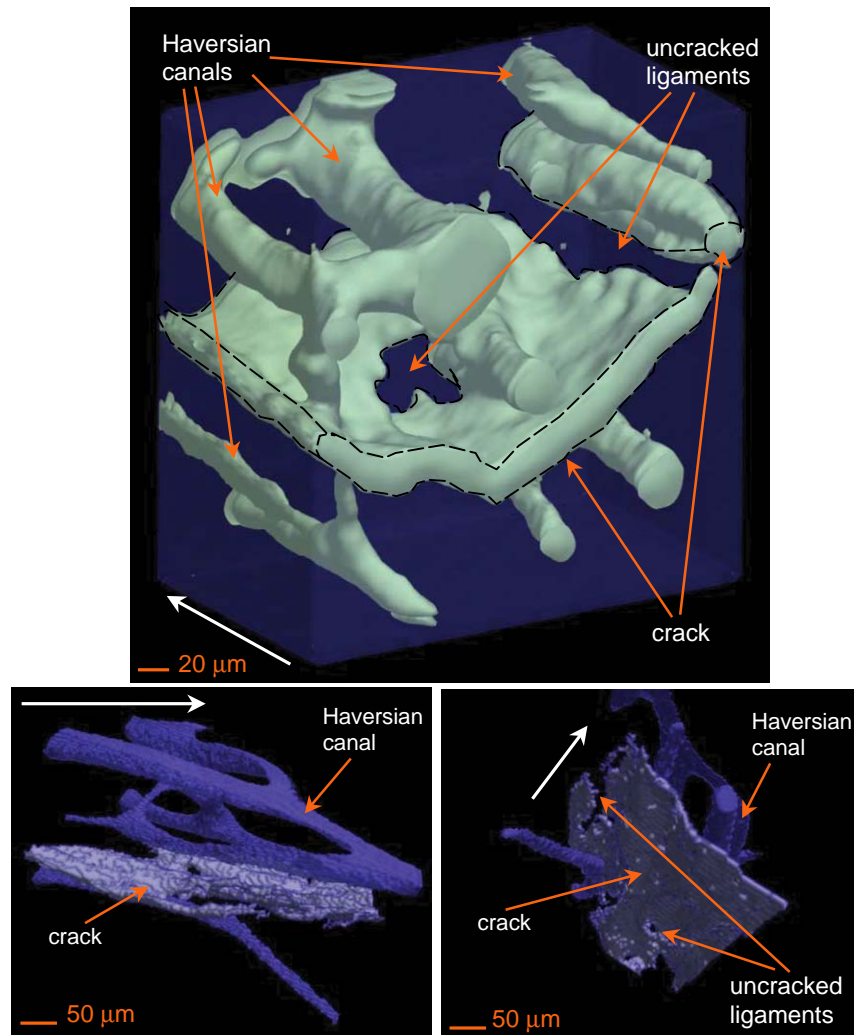


Fig. 4. Three-dimensional tomographic reconstructions of sections of the crack at a subsurface location indicated by the box in Fig. 3 (center panel). Note that the crack appears to follow the cement lines bordering the osteons. Uncracked ligaments are indicated. The white arrow in each case is the direction of nominal growth.

Table 2  
Bridging parameters for human cortical bone

Donor information <sup>a</sup>	$L$ (mm)	$K_{br}$ (MPa $\sqrt{m}$ )	$\sigma_{max}$ (Eq. (4)) (MPa)	$\sigma_{max}$ (Eq. (6)) (MPa)	$p$ (Eq. (6))
41FL#1	5.5	2.2	10.6	11.9	0.91
37ML#1	5.0	1.9	6.7	10.4	1.12
37MR#2	5.8	2.4	7.5	17.0	2.30

<sup>a</sup>The notation reads as follows: age (years), sex (M= male, F= female), arm (L=left, R=right), with any subsequent number being a unique identifier when more than one specimen were taken from the same location.

range for the three samples between 7 and 11 MPa for the stress function given by Eq. (4), and 10–17 MPa for the stress function deduced using Eq. (6).

#### 4.4. Time-dependent crack/blunting results

To determine whether bone is susceptible to subcritical cracking and/or associated crack-blunting behavior, crack growth was monitored in five C(T) samples loaded under constant displacement conditions. Based

on in situ observations, it was determined that for time scales of several hours, significant crack blunting was not observed. Instead, time-dependent cracking was observed, as shown in Fig. 7, along with a corresponding load drop with time. Accordingly, load versus time data from the constant load–line displacement tests were used to generate a crack velocity versus stress intensity, or  $da/dt-K$ , curve, shown in Fig. 8. Each data point in Fig. 8 represents a fit of the crack length versus time data over  $\sim 100 \mu\text{m}$  of crack extension, while the line

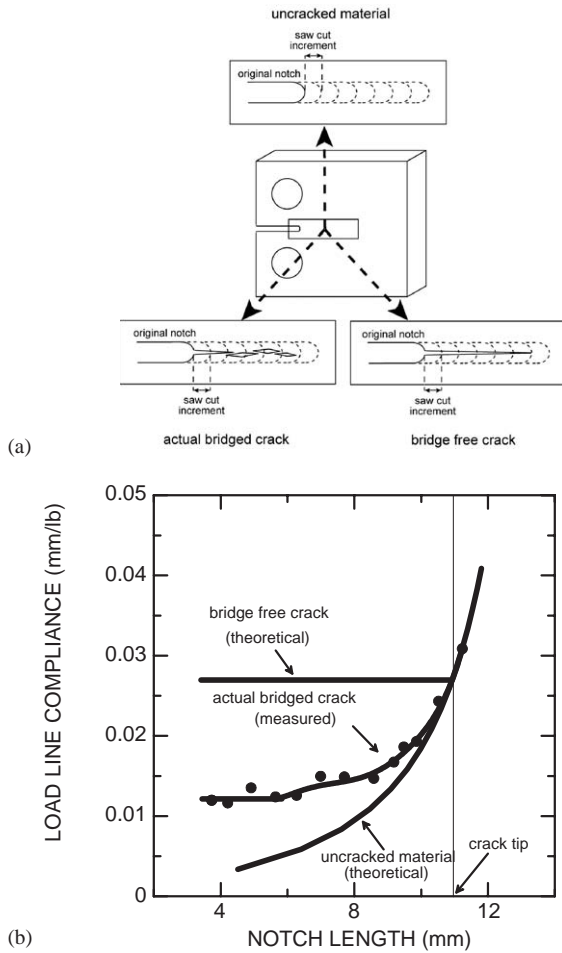


Fig. 5. Results from multi-cutting compliance experiments on a post-test specimen (41FL#1). The indicated location of the crack tip was measured by optical microscopy, while each plotted data point corresponds to the mean of five compliance measurements.

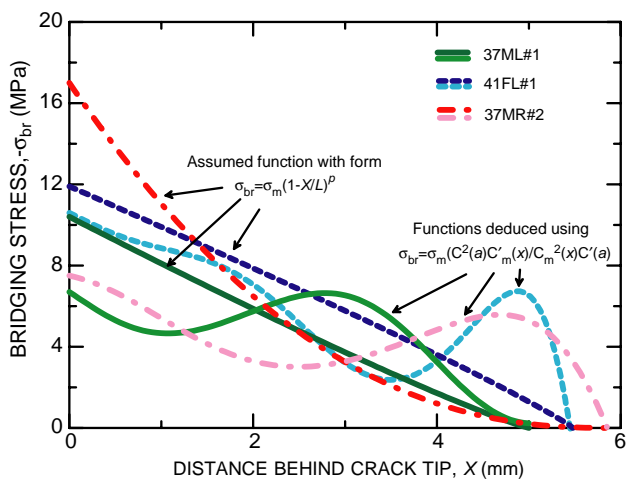


Fig. 6. Bridging stress distribution estimates for cracks in human cortical bone specimens deduced from the multi-cutting experiments.

represents a best fit to the power-law relation:

$$da/dt = AK^n, \tag{10}$$

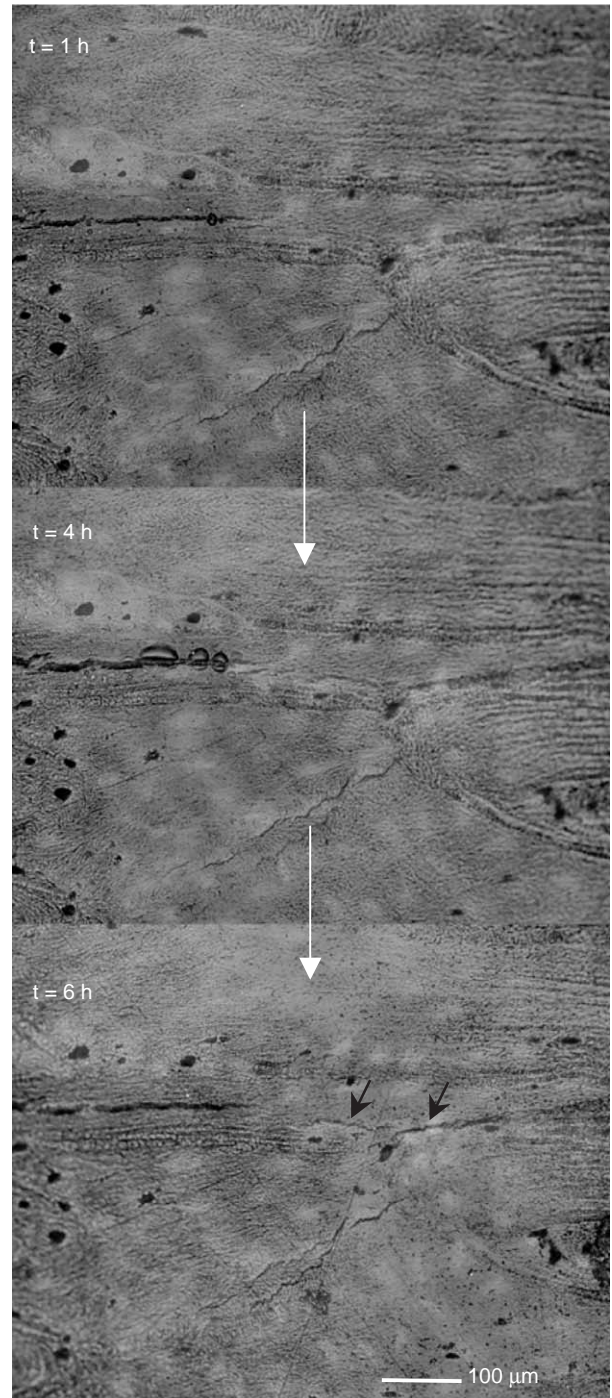


Fig. 7. Time-elapsing optical micrographs showing the time-dependent crack extension behavior (clearly seen in bottom micrograph, as indicated by black arrows) that occurs over a time scale of several hours under constant displacement conditions in human cortical bone. Note also the evidence of uncracked-ligament bridging and the lack of crack blunting on this time scale. Direction of nominal crack growth is from left to right.

where  $A$  and  $n$  are scaling constants for the power-law fit; individual values are given in Table 3.

In contrast, after holding the sample at constant displacement for several days, time-dependent crack

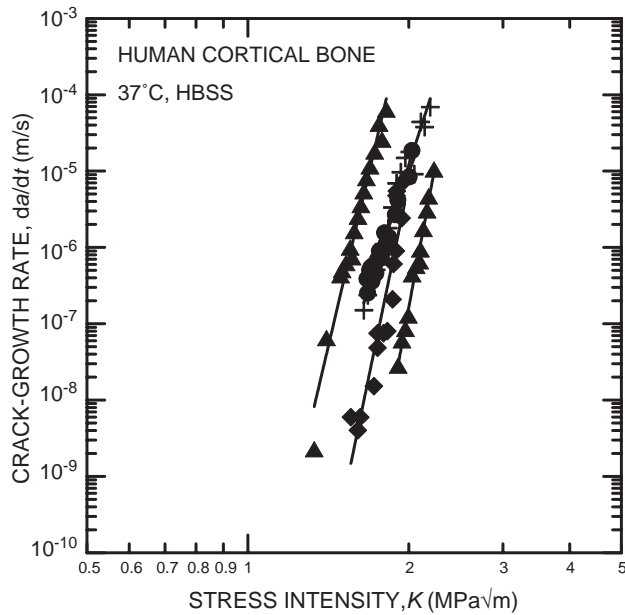


Fig. 8. Results showing the time-dependent subcritical crack-growth behavior of human cortical bone, in terms of the growth rates,  $da/dt$ , as a function of the stress intensity,  $K$ , for growth rates  $> 10^{-9}$  m/s.

blunting became evident, as seen in the time-elapsing micrographs in Fig. 9. Each micrograph in Fig. 9 was taken after the sample was unloaded to zero applied load, demonstrating the permanent plastic deformation that occurred at the crack tip. Although such blunting was not evident over the time scales used to collect the data in Fig. 8, it did interfere with attempts to collect data at lower growth rates, where test times of several days would be needed to get significant crack growth. Indeed, though there was a drop in the load on holding at constant displacement, there was practically no additional crack growth accompanying the blunting (as schematized in Fig. 1—from  $t = t_1$  to  $t = t_2$ ,  $t_2 \gg t_1$ ). The continued load drop is presumably a consequence of viscoplastic deformation processes in the vicinity of the crack tip; the exact nature of such behavior is as yet unclear.

## 5. Discussion

### 5.1. Resistance curve behavior

As noted in Section 4.1, cortical bone showed rising R-curve behavior, with an average crack-initiation toughness,  $K_0$ , of 2.03 (SD = 0.19)  $\text{MPa}\sqrt{\text{m}}$  and a mean slope of 0.39 (SD = 0.09)  $\text{MPa}\sqrt{\text{m}/\text{mm}}$  (Fig. 2b). These toughness data are slightly higher than the results of Vashishth et al. [30] for human cortical bone tested in the same proximal/distal orientation, where  $K_0$  values of  $\sim 1.6$ – $1.9$   $\text{MPa}\sqrt{\text{m}}$  and slopes of  $\sim 0.13$ – $0.27$   $\text{MPa}\sqrt{\text{m}/\text{mm}}$  were reported. These differences may be the result

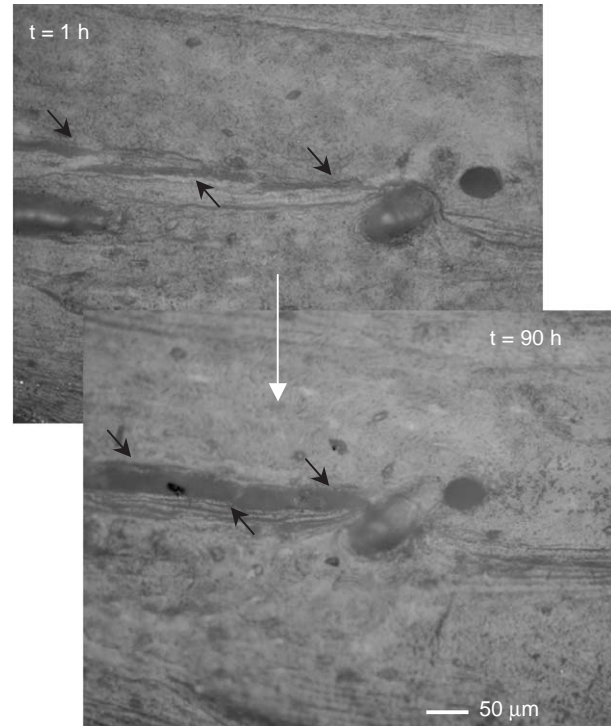


Fig. 9. Time-elapsing optical micrographs showing the time-dependent crack-tip blunting behavior that occurs over a time scale of several days (much longer than in Fig. 7) under constant displacement conditions in human cortical bone. The black arrows in each panel indicate the crack. Direction of nominal crack growth is from left to right.

of their specimens being from a different anatomical location (tibia), or (more plausibly) from older donors (59 years). Also, Malik et al. [13] reported rising R-curve behavior for transverse crack growth in equine bone, with mean  $K_0$  values of  $\sim 4.38$ – $4.72$   $\text{MPa}\sqrt{\text{m}}$ , and mean slopes (calculated from mean parameters in Ref. [13]) of  $1.06$ – $2.57$   $\text{MPa}\sqrt{\text{m}/\text{mm}}$ , depending on anatomical location; evidence of osteon pullout, crack deflection and secondary cracking was identified as the responsible mechanisms. The higher numbers in this study are presumably a result of differences in specimen orientation (transverse), donor species (horse), and anatomical location (third metacarpal bone). Furthermore, the data reported by Malik et al. [13] was qualitatively different from the data reported here and by Vashishth et al. [30]; rather than a linearly rising R-curve, these authors observed a rising portion that reached a plateau and, in some cases, decreased after that. Finally, Pezzoti and Sakakura [33] reported a rising R-curve followed by a plateau in bovine bone. They measured values of  $\sim 3.2$   $\text{MPa}\sqrt{\text{m}}$  and  $\sim 5$   $\text{MPa}\sqrt{\text{m}/\text{mm}}$  for the initiation toughness and the (initial) slope, respectively. While they did show evidence of crack bridging as the responsible toughening mechanism, the orientation of the specimens (transverse or longitudinal) was unclear.

Table 3  
Time-dependent cracking of human cortical bone

Donor information <sup>a</sup>	Prefactor, $A$ (MPa $\sqrt{m}$ ) <sup>-n</sup> m/s	Exponent, $n$	Coefficient of determination ( $R^2$ )
37ML#3	$4.8 \times 10^{-12}$	21.3	0.96
37ML#4	$2.5 \times 10^{-15}$	31.2	0.81
37MR#3	$2.2 \times 10^{-11}$	18.7	0.94
37MR#4	$7.7 \times 10^{-19}$	37.6	0.99
41FL#3	$1.6 \times 10^{-12}$	29.9	0.97
41FL#4 <sup>b</sup>	—	—	—

<sup>a</sup>The notation reads as follows: age (years), sex (M= male, F= female), arm (L=left, R=right), with any subsequent number being a unique identifier when more than one specimen were taken from the same location.

<sup>b</sup>Specimen used for in situ experiment.

## 5.2. Bridging-zone characterization

As has been reported recently for human [14,32] and bovine [33] cortical bone, the present results reaffirm the notion that crack bridging is a major toughening mechanism. New results in the present work (using X-ray tomography) clearly confirm how such bridging elements exist throughout the thickness of the specimen (Fig. 3), and (using multi-cutting compliance experiments) how they can sustain significant loads in the crack wake. The compliance-based measurements and analysis (Fig. 5) indicate that bridging zones for human cortical bone are far larger than first thought [53]; indeed, they are on the order of 5.5 mm long. These bridging zones are much longer than those inferred for hydrated dentin [31], which reached a steady-state “plateau” toughness after only ~1–2 mm. This difference is presumably due to the much lower degree of blunting, and correspondingly smaller crack-opening displacements, seen in cortical bone over the same time scales. Indeed, the larger crack openings in dentin caused bridges to be destroyed in the crack wake much more quickly than in bone.

Our experiments and analysis have allowed us to estimate some associated bridging stress distributions (Fig. 6, Table 2). Some specimen-to-specimen variations are seen, which reflect the stochastic nature of bridging and hence the scatter in the R-curves; however, the general magnitude of the bridging stresses are similar in all cases. Distributions deduced using the two different methods are also similar, although there are some obvious differences. First,  $\sigma_{\max}$  values deduced using Eq. (6) were always higher than those from Eq. (4); however, this difference is related to the more restrictive assumptions on distribution shape since it is the integral of the stress distribution which determines  $K_{br}$ . Furthermore, qualitatively it is seen in Fig. 5 that there was a jump in the compliance, followed by a plateau, before the compliance began to increase again during the multi-cutting compliance experiment. Similar results were seen for each sample, although at different locations. This corresponds to a local maximum in the bridging stress function determined using Eq. (4) for sample 41FL#1

roughly 4.8 mm behind the crack tip, which suggests that a large bridge was cut away in this region during the experiment. Such a result is consistent with X-ray tomography results (Fig. 3), which indicate that large bridges, several hundreds micrometers in size, exist behind the crack tip. Accordingly, compliance jumps associated with the cutting out of large bridges are to be expected and are reflected in the bridging function deduced using Eq. (4), while such details are lost by the use of Eq. (6), which forces a very smooth bridging stress distribution.

One previous study by Pezzotti and Sakakura [33] used Raman spectroscopy techniques to quantify the bridging stresses in bovine bone, yielding values as high as 300 MPa within the first 10  $\mu\text{m}$  of the crack tip. While it is noted that differences in bovine and human bone are likely, this alone should not account for such large discrepancies. Instead, it should be recognized that the Raman spectroscopy technique used in Ref. [33] characterized the bridging stresses on a much finer size scale, analyzing 1  $\mu\text{m}$  diameter regions on the sample surface with a penetration depth of only ~20  $\mu\text{m}$ . In contrast, the present techniques give smoothed-out averages of the bridging stress distribution both along the crack wake and through the thickness of the sample. Accordingly, local regions of very high bridging stresses, similar to those observed in Ref. [33], are not inconsistent with the present results. The lower bridging stresses deduced in the present work are merely indicative of the fact that bridges are discreet entities, and while the stresses may be very high locally, this will be offset by surrounding unbridged regions unable to support any load when considering the average through-thickness behavior. Furthermore, bridging stresses as high as 300 MPa were only found within ~10  $\mu\text{m}$  of the crack tip, while they fell off significantly to ~10–50 MPa at distances of ~100  $\mu\text{m}$  from the crack tip. Such values are more in line with the present results, which indicate average bridging stresses of ~7–17 MPa at the same position.

The calculated bridging stress intensities,  $K_{br} \sim 1.9\text{--}2.4 \text{ MPa}\sqrt{\text{m}}$ , for the specimens used in the multi-compliance cutting tests are somewhat higher than

theoretical estimates of ligament bridging based on a limiting crack-opening approach [54], where,

$$K_{br} = -f_{ul}K_I[(1 + l_{ul}/rb)^{1/2} - 1]/[1 - f_{ul} + f_{ul}(1 + l_{ul}/rb)^{1/2}]. \quad (11)$$

In Eq. (11),  $f_{ul}$  is the area fraction of bridging ligaments on the crack plane ( $\sim 0.45$ , from crack path observations<sup>5</sup>),  $K_I$  is the applied (far-field) stress intensity ( $\sim 4.5 \text{ MPa}\sqrt{\text{m}}$ ),  $l_{ul}$  is the bridging zone size ( $\sim 5 \text{ mm}$ , from the compliance measurements),  $r$  is a rotational factor (0.20–0.47) and  $b$  is the length of the remaining uncracked region ahead of the crack. Substituting typical values for these parameters, toughening of the order of  $K_{br} \sim 1\text{--}1.6 \text{ MPa}\sqrt{\text{m}}$  can be predicted, somewhat lower than the measured values, although better estimates of the area fraction of bridges are necessary for more accurate predictions. Note also that there might be an additional contribution of bridging by collagen fibers, but given the bridging zone size scales involved here, such contributions are likely to be much smaller [32,53].

### 5.3. Time-dependent behavior

Results in Fig. 8 indicate that time-dependent crack growth can in fact occur in bone under sustained (non-cyclic) in vitro loads at stress intensities lower than the nominal crack-initiation toughness,  $K_0$ , measured on the R-curve (Fig. 2). This implies that bone can fail subcritically at stresses well below those required for overload (instantaneous) fracture. Indeed, measurable crack growth was observed at stress intensities as low as  $1.33 \text{ MPa}\sqrt{\text{m}}$ , i.e., 35% lower than  $K_0$  (Fig. 8). Although the mechanism of such cracking is as yet unclear, it does imply that the fracture toughness and the R-curves alone are not sufficient to fully characterize the fracture behavior of cortical bone; some consideration must additionally be made for its time-dependent crack-growth properties.

The current experiments reveal that under constant displacement, i.e., decreasing  $K$ , conditions, cortical bone demonstrates two regimes of time-dependant behavior: an initial stable crack-growth period during the first several hours of loading, followed by the suppression of such cracking due to significant (time-dependent) crack-tip blunting (which was observed in earnest after loading for more than 1 day). Such behavior is similar to that observed in hydrated dentin, although the time scales involved are very different [31]. In dentin, crack blunting occurs quite rapidly, causing

crack arrest within the first hour, which allows very little crack extension to occur in the hydrated state under constant displacement conditions. In contrast, crack blunting occurs much more slowly in hydrated cortical bone, allowing time-dependent cracking to occur far more readily (Fig. 8). In this case, it is only at very slow growth rates (e.g.,  $< 10^{-9} \text{ m/s}$ ) that there is adequate time for significant crack blunting to suppress such cracking.

These observations imply that in mineralized tissue such as bone (and dentin) subjected to sustained loading, there is a mutual competition between time-dependent crack blunting and subcritical crack extension. At higher stress intensities, the rate of forward progress of the crack tip exceeds the blunting-induced lateral displacement of the crack sides, such that significant crack extension may be achieved, as seen in Fig. 8. At growth rates below  $\sim 10^{-9} \text{ m/s}$ , however, crack blunting becomes the more prominent mechanism; this causes the observed drop in load with time during the experiment, and leads to only limited crack extension. Thus, bone has a mechanism to arrest subcritical cracks, without the need for remodeling. In dentin, where considerable blunting occurs much more rapidly, even within the first hour [31], much higher growth rates are required to overcome the crack-blunting phenomena and sustain crack growth. That crack-tip blunting occurs more slowly in bone than in dentin is a significant finding of this study. Identifying the cause of this difference (see below) is essential for developing a microstructure-based model of crack growth and fracture, and for understanding how age-related changes in bone quality and microstructure affect fracture risk.

### 5.4. Microstructural considerations

As mentioned above, the time-dependent crack growth behavior reported for hydrated cortical bone in this study is in sharp contrast with that reported for hydrated dentin in a previous study [31]. This is very surprising because at molecular and nanoscale dimensions, bone and dentin are quite similar, and are composed of type-I collagen fibrils reinforced with nanocrystalline apatite mineral. In bone, the collagen is organized into lamellae, with a more complex hierarchical structure than in dentin, where the collagen forms a simple scaffold oriented perpendicular to the dentinal tubules (i.e., the path taken by the odontoblasts during the formative stages). Accordingly, it is convenient to assume that, at this length scale, the mechanical properties of bone and dentin are similar; consequently, dentin could be expected to be a simpler structural analog for bone without the added complexity of the hierarchical microstructure. This fundamental similarity is reflected in the rising R-curve behavior (explained in terms of uncracked-ligament bridging) and

<sup>5</sup>The area fraction of 0.45 used in this calculation is an average of the range of values observed (0.15–0.75). The actual area fraction varied with location, with values as high as 0.5–0.75 near the crack tip and as low as 0.15–0.25 a few mm behind the crack tip; such variations are currently being imaged and investigated.

the presence of time-dependent crack growth in both tissues. However, important differences crop up when the time scales for crack blunting are considered. A plausible explanation for these differences can be found without abandoning our assumption, if we focus on differences in the microstructure of the two tissues at longer length scales.

One such distinctive feature in the microstructure of bone that adds to its complexity is the osteon, and in particular, the cement line at the boundary separating the osteons from the surrounding (primary) lamellar bone. As observed in the optical micrographs, and confirmed in the three-dimensional tomography images (Figs. 3 and 4), the advancing crack never penetrated the osteons. Rather, the crack deflected around the osteons, propagating preferentially along the presumably weaker cement line. It is possible that the cement line fails ahead of the advancing crack, and links back up with the main crack through the intervening tissue. This process of linking up would keep the advancing crack tip sharp and would also support the formation of uncracked ligaments in the wake of the crack where full linking back has not been achieved. Only at lower stresses, where the cement line remains intact ahead of the advancing crack, is there sufficient time for crack-tip blunting to occur. The exact microstructural mechanism of time-dependent blunting is as yet unclear, and could involve both the collagen fibrils and the surrounding matrix, similar to what has been suggested to explain viscoelastic behavior in rat-tail tendon [55]. As yet, this hypothesis that the additional microstructural complexity introduced by the cement line in cortical bone is responsible for the different time-dependent behavior is speculative and will require further study. In principle, it might be possible to test the assumption in a different tissue, like rat bone, which has a Haversian system, but does not undergo osteonal remodeling and the cement line would therefore be absent. Understanding the behavior of the cement line gains added significance when viewed in conjunction with variables like microstructural orientation, aging and remodeling.

With regards to the role of orientation of the microstructure in cortical bone, the present study admittedly has been limited to crack growth in the proximal–distal orientation. However, a similar effect of the cement line *locally* “deflecting” the crack was observed for crack growth in a radial direction (e.g., medial–lateral) [14,53]. For crack growth in a transverse orientation, the cement line has been known to cause *global* (out-of-plane) crack deflection as reflected in the much higher toughness in that orientation [8,14,56]. However, if the crack in this orientation were constrained to remain within the proximal–lateral plane (as can be achieved by side grooving the test specimen, e.g. [56–58]), the crack would be forced to cut through the entire osteon (and not deflect away along the cement

line), and it is plausible that this could lead to enhanced blunting. This is currently under investigation.

Finally, in order to eliminate the added complexity introduced by aging-related changes, the present study has also been intentionally restricted to a rather narrow donor age group (34–41 years). There are a large number of studies in archival literature that have looked at age-related issues in the mechanical properties of bone (e.g., [11,25,59–61]), and have suggested a significant deterioration of the fracture toughness with age. In particular, aging has been associated with lowered collagen network integrity, with resultant reduction in the toughness [11], presumably due to poorer quality uncracked-ligament bridges being formed. Also, it has been suggested that remodeling induced by increasing microdamage with aging [62] leads to an increase in the difference in properties of the matrix (primary lamellar bone) and the secondary osteons, implying a stronger role for the cement lines and a reduction in the toughness [8,25,60]. Clearly, further investigations are needed to assess how such changes affect the microstructure of bone at various levels, and their resultant effect on the mechanisms of toughening. Such an approach is fundamental to furthering our understanding of the effects of aging on the fracture properties of mineralized tissues.

## 6. Conclusions

Based on a study of the *in vitro* fracture toughness behavior of hydrated human cortical bone in Hanks' Balanced Salt Solution, the following conclusions can be made:

1. The fracture toughness behavior of cortical bone can be displayed in terms of rising resistance-curve (R-curve) behavior, consistent with previous studies. This behavior can be attributed to crack-tip shielding. The primary source of such shielding was due to the formation of uncracked-ligament bridges in the crack wake.
2. Subsurface examination of crack paths using computed X-ray tomography indicated that such bridges are essentially two-dimensional in nature, but persist throughout the thickness of the specimens; they are not merely surface features.
3. Multi-cutting compliance experiments revealed that the bridging zone extends for some 5 mm or so behind the crack tip of a growing crack in human cortical bone. Additionally, the compliance results were used to derive quantitative estimates for the bridging stress distribution in the crack wake.
4. Human cortical bone was shown to be susceptible to time-dependent subcritical cracking at (non-cyclic) stresses well below that required for instantaneous

fracture. Indeed, such crack-growth behavior was observed at stress intensities as low as 35% below the crack-initiation toughness,  $K_0$ , on the R-curve.

5. For a growing crack under constant displacement (decreasing  $K$ ) conditions in human cortical bone, there appears to be a mutual competition between such subcritical cracking and significant crack-tip blunting. At higher driving forces and growth rates ( $da/dt > 10^{-9}$  m/s), subcritical cracking occurred more readily, whereas at slower crack growth rates ( $da/dt < 10^{-9}$  m/s), time-dependent blunting becomes dominant to the point that crack growth is effectively suppressed.
6. The fact that cracks in cortical bone undergo blunting over time scales that are much longer than in dentin, despite having a similar structure (collagen fibrils reinforced with nanocrystalline apatite) at the nanoscale, is related to differences in their structures at coarser dimensions, specifically with respect to the presence of the osteons in bone. Cracks in bone tend to deflect around the osteons and propagate preferentially along the weaker cement lines, which act to keep the crack tip sharp.

## Acknowledgements

This work was supported by the National Institutes of Health under Grant No. 5RO1 DE015633 (for RKN and JHK) and by the Director, Office of Science, Office of Basic Energy Science, Division of Materials Sciences and Engineering, Department of Energy under Contract No. DE-AC03-76SF00098 (for JJK and ROR). We also acknowledge the support of the Stanford Synchrotron Radiation Laboratory (SSRL), supported by Department of Energy Contract No. DE-AC03-76SF00515, and wish to thank David Haupt for assistance with the tomography, Dr. A.P. Tomsia for his support, and Drs. C. Puttlitz and Z. Xu for supply of the cortical bone.

## References

- [1] Heaney R. Is the paradigm shifting? *Bone* 2003;33:457–65.
- [2] Yeni YN, Brown CU, Wang Z, Norman TL. The influence of bone morphology on fracture toughness of the human femur and tibia. *Bone* 1997;21:453–9.
- [3] Rho J-Y, Kuhn-Spearing L, Zioupos P. Mechanical properties and the hierarchical structure of bone. *Med Eng Phys* 1998;20:92–102.
- [4] Weiner S, Wagner HD. The material bone: structure–mechanical function relations. *Annu Rev Mater Sci* 1998;28:271–98.
- [5] Braidotti P, Bemporad E, D'Alessio T, Sciuto SA, Stagni L. Tensile experiments and SEM fractography on bovine subchondral bone. *J Biomech* 2000;33:1153–7.
- [6] Reilly GC, Currey JD. The effects of damage and microcracking on the impact strength of bone. *J Biomech* 2000;33:337–43.
- [7] Vashishth D, Tanner KE, Bonfield W. Contribution, development and morphology of microcracking in cortical bone during crack propagation. *J Biomech* 2000;33:1169–74.
- [8] Yeni YN, Norman TL. Calculation of porosity and osteonal cement line effects on the effective fracture toughness of cortical bone in longitudinal crack growth. *J Biomed Mater Res* 2000;51:504–9.
- [9] Parsamian GP, Norman TL. Diffuse damage accumulation in the fracture process zone of human cortical bone specimens and its influence on fracture toughness. *J Mater Sci: Mater Med* 2001;12:779–83.
- [10] Wang X, Bank R, Tekoppele J, Agrawal C. The role of collagen in determining bone mechanical properties. *J Orthop Res* 2001;19:1021–6.
- [11] Wang X, Shen X, Li X, Agrawal CM. Age-related changes in the collagen network and toughness of bone. *Bone* 2002;31:1–7.
- [12] Hiller LP, Stover SM, Gibson VA, Gibeling JC, Prater CS, Hazelwood SJ, Yeh OC, Martin RB. Osteon pullout in the equine third metacarpal bone: effects of ex vivo fatigue. *J Orthop Res* 2003;21:481–8.
- [13] Malik CL, Stover SM, Martin RB, Gibeling JC. Equine cortical bone exhibits rising R-curve fracture mechanics. *J Biomech* 2003;36:191–8.
- [14] Nalla RK, Kinney JH, Ritchie RO. Mechanistic fracture criteria for the failure of human cortical bone. *Nat Mater* 2003;2:164–8.
- [15] O'Brien FJ, Taylor D, Lee TC. Microcrack accumulation at different intervals during fatigue testing of compact bone. *J Biomech* 2003;36:973–80.
- [16] Vashishth D, Tanner KE, Bonfield W. Experimental validation of a microcracking-based toughening mechanism for cortical bone. *J Biomech* 2003;36:121–4.
- [17] Yeni YN, Brown CU, Norman TL. Influence of bone composition and apparent density on fracture toughness of the human femur and tibia. *Bone* 1998;22:79–84.
- [18] Yeni YN, Norman TL. Fracture toughness of human femoral neck: effect of microstructure, composition, and age. *Bone* 2000;26:499–504.
- [19] Currey JD. 'Osteons' in biomechanical literature. *J Biomech* 1982;15:717.
- [20] Knott JF. *Fundamentals of fracture mechanics*. London, UK: Butterworth & Co. (Publishers) Ltd; 1976.
- [21] Bonfield W. Advances in the fracture mechanics of cortical bone. *J Biomech* 1987;20:1071–81.
- [22] Lucksanabool P, Higgs WAJ, Higgs RJED, Swain MW. Fracture toughness of bovine bone: influence of orientation and storage media. *Biomaterials* 2001;22:3127–32.
- [23] Norman TL, Vashishth D, Burr DB. Fracture toughness of human bone under tension. *J Biomech* 1995;28:309–20.
- [24] Brown CU, Yeni YN, Norman TL. Fracture toughness is dependent on bone location- A study of the femoral neck, femoral shaft, and the tibial shaft. *J Biomed Mater Res* 2000;49:380–9.
- [25] Phelps JB, Hubbard GB, Wang X, Agrawal CM. Microstructural heterogeneity and the fracture toughness of bone. *J Biomed Mater Res* 2000;51:735–41.
- [26] Lawn BR. Physics of fracture. *J Am Ceram Soc* 1983;66:83.
- [27] Ritchie RO. Mechanisms of fatigue crack propagation in metals, ceramics and composites: role of crack-tip shielding. *Mater Sci Eng* 1988;103:15–28.
- [28] Ritchie RO. Mechanisms of fatigue-crack propagation in ductile and brittle solids. *Int J Fract* 1999;100:55–83.
- [29] Evans AG. Perspective on the development of high toughness ceramics. *J Am Ceram Soc* 1990;73:187–206.
- [30] Vashishth D, Behiri JC, Bonfield W. Crack growth resistance in cortical bone: concept of microcrack toughening. *J Biomech* 1997;30:763–9.

- [31] Kruzic JJ, Nalla RK, Kinney JH, Ritchie RO. Crack blunting, crack bridging and resistance-curve fracture mechanics in dentin: effect of hydration. *Biomaterials* 2003;24:5209–21.
- [32] Nalla RK, Kruzic JJ, Ritchie RO. On the origin of the toughness of mineralized tissue: microcracking or crack bridging? *Bone*, in press.
- [33] Pezzotti G, Sakakura S. Study of the toughening mechanisms in bone and biomimetic hydroxyapatite materials using Raman microprobe spectroscopy. *J Biomed Mater Res* 2003;65A:229–36.
- [34] Kahler B, Swain MV, Moule A. Fracture-toughening mechanisms responsible for differences in work of fracture of hydrated and dehydrated dentine. *J Biomech* 2003;36:229–37.
- [35] Nalla RK, Kinney JH, Ritchie RO. Effect of orientation on the in vitro fracture toughness of dentin: the role of toughening mechanisms. *Biomaterials* 2003;24:3955–68.
- [36] Habelitz S, Marshall GW, Balooch M, Marshall SJ. Nanoindentation and the storage of teeth. *J Biomech* 2002;35:995–8.
- [37] Saxena A, Hudak Jr SJ. Review and extension of compliance information for common crack growth specimens. *Int J Fract* 1978;14:453–68.
- [38] Kinney JH, Nichols MC. X-ray tomographic microscopy (XTM) using synchrotron radiation. *Annu Rev Mater Sci* 1992;22: 121–52.
- [39] Hu X, Wittmann FH. Experimental method to determine extension of fracture-process zone. *J Mater Civil Eng* 1990;2:15–23.
- [40] Hu X-Z, Wittmann FH. Fracture process zone and K<sub>r</sub>-curve of hardened cement paste and mortar. In: Shah SP, Swartz SE, Barr B, editors. *Fracture of concrete and rock: Recent developments*. University of Wales, College of Cardiff, London, UK: Elsevier; 1989.
- [41] Wittmann FH, Hu X. Fracture process zone in cementitious materials. *Int J Fract* 1991;51:3–18.
- [42] Ballarini R, Shah SP, Keer LM. Crack growth in cement-based composites. *Eng Fract Mech* 1984;20:433–45.
- [43] Wecharatana M, Shah SP. A model for predicting fracture resistance in reinforced concrete. *Cement Concrete Res* 1983;13:819–29.
- [44] Hu X-Z, Lutz EH, Swain MV. Crack-tip-bridging stresses in ceramic materials. *J Am Ceram Soc* 1991;74:1828–32.
- [45] Foote RML, Mai Y-M, Cotterell B. Crack growth resistance curves in strain-softening materials. *J Mech Phys Solids* 1986;34:593–607.
- [46] Mai Y-W, Lawn BR. Crack-interface grain bridging as a fracture resistance mechanism in ceramics: II, theoretical fracture mechanics model. *J Am Ceram Soc* 1987;70:289–94.
- [47] Bueckner HF. A novel principle for the computation of stress intensity factors. *Z Angew Math Mech* 1970;50:529–46.
- [48] Fett T, Munz D. *Stress intensity factors and weight functions*. Southampton, UK: Computational Mechanics Publications; 1997. p. 408.
- [49] An YH. *Mechanical properties of bone, in mechanical testing of bone and the bone-implant interface*. Boca Raton, FL: CRC Press; 2000. p. 41–63.
- [50] Suresh S. *Fatigue of materials*, 2nd ed. Cambridge, UK: Cambridge University Press; 1998.
- [51] Behiri JC, Bonefield W. Fracture mechanics of bone—the effects of density, specimen thickness, and crack velocity on longitudinal fracture. *J Biomech* 1984;17:25–34.
- [52] Cox BN. Extrinsic factor in the mechanics of bridged cracks. *Acta Metall Mater* 1991;39:1189–201.
- [53] Nalla RK, Stölken JS, Kinney JH, Ritchie RO. On the micro-mechanisms of in vitro fracture and toughening in human cortical bone. *J Biomech*, in review.
- [54] Shang JK, Ritchie RO. Crack bridging by uncracked ligaments during fatigue-crack growth in SiC-reinforced aluminum-alloy composites. *Metall Trans A* 1989;20A:897–908.
- [55] Puxkandl R, Zizak I, Paris O, Keckes J, Tesch W, Bernstorff S, Purslow P, Fratzl P. Viscoelastic properties of collagen: synchrotron radiation investigations and structural model. *Philos Trans R Soc London B: Biol Sci* 2002;357:191–7.
- [56] Behiri JC, Bonefield W. Orientation dependence of the fracture mechanics of cortical bone. *J Biomech* 1989;22:863–72.
- [57] Malik CL, Gibeling JC, Martin RB, Stover SM. Compliance calibration for fracture testing of equine cortical bone. *J Biomech* 2002;35:701–5.
- [58] Gibeling JC, Shelton DR, Malik CL. Application of fracture mechanics to the study of crack propagation in bone. In: *Structural biomaterials for the 21st century*. Warrendale, PA: TMS; 2001.
- [59] Burstein A, Reilly D, Martens M. Aging of bone tissue mechanical properties. *J Bone Joint Surg* 1976;58A:82–6.
- [60] Zioupos P, Currey JD. Changes in the stiffness, strength, and toughness of human cortical bone with age. *Bone* 1998;22:57–66.
- [61] Zioupos P, Currey JD, Hamer AJ. The role of collagen in the declining mechanical properties of aging human cortical bone. *J Biomed Mater Res* 1999;2:108–16.
- [62] Lee TC, Staines A, Taylor D. Bone adaptation to load: microdamage as a stimulus for bone remodelling. *J Anat* 2002;201:437–46.